Wärme- und Stoffübertragung 6 (1973) 69–77

Spot Formation at the Anode of High Intensity Arcs

T. S. CHOU, St. Petersburg, Florida and E. PFENDER, Minneapolis, Minnesota

Abstract. A simple analytical model is proposed which describes the region between a plane, cooled nonablating anode and an arc column normal to the anode. The model takes an initial arc contraction into account due to the low temperature of the anode ("thermal pinch"). The resulting magnetic pinch effect leads to an entrainment of cold gas which determines via an energy balance the final shape of the arc in the anode region. The conservation equations are solved numerically for the anode region with a relaxation method, and results are presented based on atmospheric arcs in nitrogen. Finally, limitations of this model and necessary refinements are briefly discussed; possible extensions of the arc parameter range for future work are proposed.

Zusammenfassung. Es wird ein vereinfachtes analytisches Modell vorgeschlagen, das eine Beschreibung der Zone zwischen einer ebenen, gekühlten, nicht verdampfenden Anode und einer senkrecht dazu brennenden Bogensäule gestattet. Dieses Modell zieht eine anfängliche Einschnürung des Lichtbogens, die durch die niedrige Anodentemperatur verursacht wird, in Betracht („Thermischer Pincheffekt"). Der daraus folgende magnetische Pincheffekt saugt kaltes Gas an und die entsprechende thermische Bilanz bestimmt dann die endgültige Form des Lichtbogens im Anodengebiet. Die Erhaltungsgleichungen werden für das Anodengebiet mit einer Relaxationsmethode numerisch gelöst und Ergebnisse, die sich auf einen Stickstoffbogen bei Atmosphärendruck beziehen, werden dargestellt. Schließlich werden die begrenzte Gültigkeit dieses Modells und notwendige Verbesserungen kurz diskutiert. Mögliche Ausweitungen des Lichtbogenparameterbereichs für zukünftige Arbeiten werden ebenfalls erwähnt.

Nomenclature

A, B, C, D	refers to surfaces in Fig. 2
a, b	abbreviations defined in conjunction with Eq. (5)
c	velocity of light
E	electric field strength
F	Lorentz force per unit volume
H	self-magnetic field
h	enthalpy
I	arc current
j	current density
k	heat conductivity
p	pressure
R	radius
r	radial coordinate
T	temperature
T_1	$= T(z_b, r \geqslant R_a)$
u	component of the velocity vector in z-direction
$\bar{v}$	velocity vector
v	component of the velocity vector in r-direction
z	axial coordinate
γ	slope factor
ϕ	electrical potential
σ	electrical conductivity
ρ	density
ξ	dummy variable
Subscripts	
a	refers to surface A
b	refers to surface B
col	refers to the undisturbed arc column
cr	critical
d	refers to surface D
w	refers to the wall of the constrictor tube
0	refers to the axis (r = 0)

1. Introduction

Although high intensity arcs have been widely used in the laboratory as well as in commercial applications during the past twenty years, their electrode regions are still poorly understood. There is, for example, no consistent quantitative theory of the anode region available which permits a complete interpretation of the observed anode phenomena.

The only attempt so far to formulate an anode fall theory has been made by Bez and Höcker [1, 2]. In this theory they consider a one-dimensional model region between the plasma column and the anode in which the arc contracts toward the anode surface and in which the necessary ions are generated. Assuming Maxwellian velocity distributions for all species and using the concept of mobility, they arrive at a system of equations for the drift and the thermal velocities of the electrons and the ions. From an energy balance, an additional equation is derived which permits determination of current densities. Since the total current is constant in all cross sections, this equation is then used to determine the arc periphery of the contraction region.

Based on this model, Chou [3] rigorously calculated the contraction in front of the anode for an atmospheric

arc in air. The results show a severe contraction of the arc over an extremely short distance from the anode surface. This is physically not realistic and, in addition, excludes a one-dimensional treatment of the anode region. The specification of realistic boundary conditions at the edge of the sheath (the sheath separates the plasma from the anode surface) is a necessary prerequisite for calculations of the anode fall. Such boundary conditions may be obtained from an analysis of the contraction region which extends far beyond the sheath into the plasma. There is no doubt that these boundary conditions will substantially deviate from the "free stream" properties of the plasma.

The similarities between cathode and anode region of high intensity arcs justifies a brief discussion of some of the numerous efforts for analyzing the cathode region. This region has been treated comprehensively by Ecker [4–6]. He subdivides the cathode region into three model zones–the contraction, space charge, and surface zone, specifying matching boundary conditions to form a self-consistent model. He assumes that the contraction is confined to the contraction region in which quasi-equilibrium and quasi-neutrality prevail. Solutions of the conservation equations combined with Maxwell's equations are obtained for the cathode region employing the previously-mentioned boundary conditions.

Although the magnetic pinch effect is negligible for typical high intensity arcs (arc currents in the order of 100 amps), the cathode jet induced by the interaction of the arc current with the self-magnetic field may have an appreciable effect on the observed constriction. The convective heat transfer due to the induced flow represents an important term in the energy balance which, in turn, governs the degree of constriction.

In more recent studies, Lee, et al. [7, 8] extensively investigated the cathode region adopting Ecker's three zone model. In addition, they subdivide the space charge region into four subregions and make a thorough investigation of them and the entire one-dimensional region as a whole. They assume a realistic cathode jet flow pattern and take convective heat transfer into account which has been neglected in previous analyses [4–6].

The model proposed for this study takes an initial constriction of the arc adjacent to the anode into account. This initial constriction results from a thermal analysis of the anode region excluding any flow effects.

The jet flow can be obtained by a solution of the momentum equations. At this time, it is felt that such a solution is not necessary. The effect of the jet may be described by a simplified flow pattern without altering the essentials of the final solution.

The analysis of the entire anode region starts with the investigation of the contraction region since the conditions can be readily obtained in the plasma column. The unknown boundary condition between contraction zone and sheath can be treated as a parameter which may be matched with the values obtained from a later analysis of the space charge region. Since the space charge region is excluded from this study, reasonable values are assumed for this boundary condition. The problem will be approached in a general manner, and comparisons will be made with experimental observations.

The model will be applied to atmospheric high intensity arcs in nitrogen. Of special interest is the effect of the total current on the contraction. Thus, calculations with three different currents will be performed. As the results will show, for the current range investigated increasing currents create slightly stronger constriction in agreement with experimental observations.

2. The Analytical Model

The proposed model is based on a rotationally symmetric arc shown schematically in Fig. 1. The axis of the arc is normal to the plane anode and the arc column is confined by a coaxial cooled constrictor tube. Similar to the cathode region described in [4–8], the anode region is subdivided into three distinctively different zones–the contraction, space charge, and the anode surface zone.

In the plasma column, a comparatively moderate current density is maintained by a uniform electric field. The energy dissipated in a volume element is transferred to the constrictor tube mainly by heat conduction. The arc is assumed to be fully developed with exception of the electrode region. Thus, the current density, the heat generation per unit volume, and the gas temperature are functions of the radius only. Consequently, there is no heat conduction in axial direction; and the plasma column can thus be analyzed one-dimensionally. From Fourier's law of heat conduction [9], follows that the gas temperature peaks on the axis and drops continuously to the temperature of the constrictor tube.

Gases are poor electrical conductors until they reach a certain temperature above which the electrical conductivity increases sharply with temperature. In the

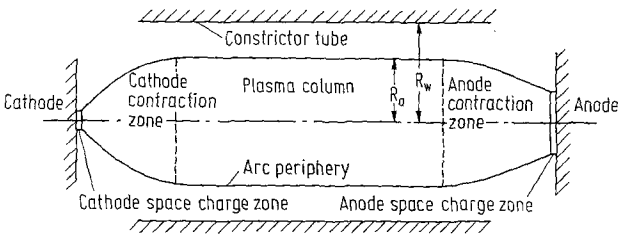

Fig. 1. Schematic of an Axisymmetric Arc with Electrode Regions

following, this temperature will be denoted as the "critical temperature". Since the temperature decreases rapidly with increasing distance from the axis of the arc column, the current is confined to a well-defined cylinder as shown in Fig. 1. The surface of this cylinder is an isothermal surface corresponding to the "critical temperature". The temperature and the current density distributions are obtained from an analysis of this one-dimensional arc model.

As the anode surface is approached, energy is lost by heat conduction in axial as well as in radial direction. This causes the surrounding gas temperature to drop and consequently forces the arc periphery to move toward the axis. It will be shown that the arc periphery can be derived from a numerical calculation which demonstrates that the relatively low temperature of the anode gives rise to this initial contraction in the anode region ("thermal pinch").

As the arc contracts, both the current density and the field strength increase. This results in a much higher heat generation rate per unit volume and consequently in very high temperatures in the core area because the increased heat dissipation is only partially offset by the higher radial heat conduction losses caused by the steeper temperature gradients. Radiation losses are neglected, although a more sophisticated model must include such losses.

The interaction of the self-magnetic field with the arc current produces a force acting on the plasma in radial direction toward the axis. This force is balanced by a pressure gradient in that direction. The plasma remains undisturbed as long as the resulting pressure distribution does not have an axial gradient as, for example, in the case of a plasma column of constant diameter. In the contraction region, however, the magnetic body force increases because of both the higher current density and the smaller arc diameter, generating a pressure gradient in axial direction pointing towards the anode. This unbalanced pressure gradient induces a flow in the core region towards the arc column, generating an anode plasma jet.

The requirement of mass conservation leads to an entrainment of gas from the surrounding area of the anode, and this gas is heated and accelerated towards the core of the arc. The cooling effect caused by this incoming cold gas reduces the temperature in the area around the arc periphery in the anode region and thus shifts the arc periphery further toward the axis. As a consequence of this additional contraction, the current density and the self-magnetic field increase further generating an even stronger anode jet. This seemingly unstable constriction mechanism is finally balanced by the increasing temperature gradient and the associated heat conduction which tends to enlarge the arc diameter. Although the initial constriction due to the low temperature of the anode may be of minor importance, this effect triggers, according to the proposed model, a much more effective constriction mechanism which may finally result in an anode spot.

Fig. 2 shows an enlarged schematic diagram of the anode contraction region with a coordinate system and other relevant notations. The boundary conditions are to be prescribed on the following surfaces:

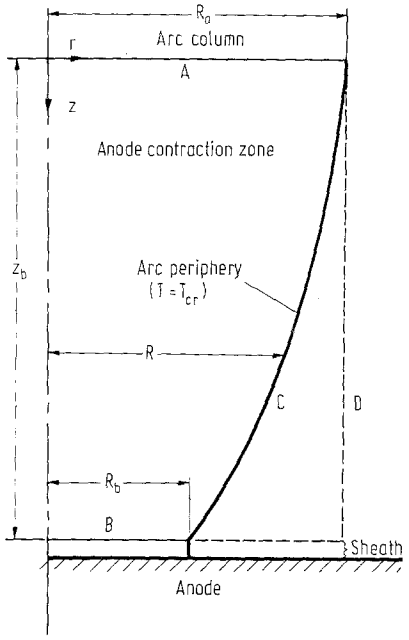

Fig. 2. Schematic Diagram of the Anode Contraction Region

A) The interface between arc column and anode contraction region.

B) The interface between anode contraction region and anode sheath.

C) The arc periphery in the anode contraction region.

D) The circular cylindrical surface extending from the periphery of the undisturbed arc column. This surface has been chosen because the thermal and the electrical boundary conditions can be reasonably well prescribed along this surface.

The following assumptions are made in connection with the adopted model:

1. Steady state prevails.
2. Local thermodynamic equilibrium exists in the contraction zone.
3. Heat transfer by radiation is negligible.
4. Heat generation due to viscosity is negligible.
5. The temperature distribution on A is the same as in the undisturbed arc column, and the potential is uniform over this surface.
6. The thickness of the region, z_b, is in the order of 1 mm.
7. The axial temperature gradient on surface B is assumed to follow a parabolic function dropping from zero on the axis to negative values. Along the circle of intersection between surfaces B and D, this negative

value shall be compatible with the temperature gradient of surface D.

8. The current density profile on surface B shall be similar to that on surface A.

9. No current flows outside of the arc periphery, i.e., anywhere outside of surface C.

10. The temperature distribution on surface D is assumed in the form of a third degree polynomial that satisfies the conditions that $T(z_b, R_a) = T_1$, the assumed low temperature in the vicinity of the anode.

Under the above assumptions, the energy equation reduces to

$$\operatorname{div}(k \operatorname{grad} T) - \rho \bar{v} \cdot \operatorname{grad} h + \bar{j} \cdot \bar{E} = 0 \tag{1}$$

The flow velocity, $\bar{v}$, will be considered in the next section. From current conservation follows

$$\operatorname{div} \bar{j} = 0 \tag{2}$$

where

$$\bar{j} = -\sigma \operatorname{grad} \phi \tag{3}$$

since the induced field $\frac{1}{c} \bar{v} \times \bar{H}$ is small compared with the applied field.

The temperature distribution on surface A is obtained from an analysis of the arc column using the well-known column theory [10]. The remaining thermal boundary conditions are for surface B

$$\frac{\partial T}{\partial z}(z_b, r) = \left(\frac{r}{R_a}\right)^2 \frac{\partial T}{\partial z}(z_b, R_a) \tag{4}$$

and for surface D

$$T(z, R_a) = T_{cr} - a\left(\frac{z}{z_b}\right)^2 + b\left(\frac{z}{z_b}\right)^3 \tag{5}$$

where

$$a = (T_{cr} - T_1)(3 - 2\gamma)$$

and

$$b = 2(T_{cr} - T_1)(1 - \gamma) .$$

γ is a slope factor [3] $(0 < \gamma < 1)$.

In addition, there are three electrical boundary conditions. The potential, ϕ, will be specified with reference to the plane $z = 0$, so that

$$\phi(0, r) = 0 . \tag{6}$$

The assumed similarity of the current density profiles yields

$$j\left(z_b, \frac{r}{R_b}\right) = j\left(0, \frac{r}{R_a}\right) \cdot \left(\frac{R_a}{R_b}\right)^2 \tag{7}$$

Finally, $j = 0$ for $r > R$.

3. The Flow Field and the Anode Jet

The Lorentz force exerted on the plasma per unit volume by the self-magnetic field is given by

$$\bar{F} = \frac{1}{c}(\bar{j} \times \bar{H})$$

where

$$\operatorname{Curl} \bar{H} = \frac{4\pi}{c} \bar{j} .$$

For rotational symmetry, the magnetic field at any location r can be expressed by

$$H = \frac{4\pi}{c} \frac{1}{r} \int_0^r j \xi \, d\xi$$

and the corresponding Lorentz force is then

$$F(r) = \frac{4\pi}{c^2} \frac{j}{r} \int_0^r j \xi \, d\xi .$$

Neglecting gravitational forces, which are much smaller than the magnetic forces in the contraction region, the following momentum equation is obtained [10]

$$\rho \frac{d\bar{v}}{dt} = -\operatorname{grad} p + \bar{F} .$$

Combining the last two equations, the momentum equations for the z and r direction, respectively, may be written as

$$\rho\left(u \frac{\partial u}{\partial z} + v \frac{\partial u}{\partial r}\right) = -\frac{\partial p}{\partial z} \tag{8}$$

and

$$\rho\left(u \frac{\partial v}{\partial z} + v \frac{\partial v}{\partial r}\right) = -\frac{\partial p}{\partial r} + \frac{4\pi}{c^2} \frac{j}{r} \int_0^r j \xi \, d\xi \tag{9}$$

where u is the negative z-component of the velocity vector and v the corresponding negative r-component.

The continuity equation for this case is given by

$$\operatorname{div}(\rho \bar{v}) = 0 . \tag{10}$$

A rigorous solution of the flow field could be obtained by solving Eqs. (8) through (10) with appropriate boundary conditions. Such a solution, however, requires boundary conditions which can only be obtained from an extensive analysis of the surrounding

region. An approximate pattern of the flow field may, however, be obtained by the following procedure:

1. On the arc axis, v and $\partial v/\partial z$ vanish and $\partial v/\partial r$ and u are both finite so that the left-hand side of Eq. (9) becomes zero along the arc axis. This permits calculation of the pressure distribution along the arc axis assuming that atmospheric pressure prevails on surface D.

2. On the centerline, the radial velocity component v is zero and $\partial u/\partial r$ finite; therefore, with the pressure distribution known, Eq. (8) can be solved for the axial velocity component u.

3. For each axial location, the axial mass flux component, ρu, decreases monotonically from the z-axis to zero somewhere in the arc region. As a first approximation, the component ρu will be assumed as a parabolic function decreasing to zero on surface $r = R_b$, i.e.,

$$\rho(z, r)\, u(z, r) = \rho(z, 0)\, u(z, 0) \left[1 - \left(\frac{r}{R_b}\right)^2\right] \quad \text{for } r < R_b \qquad (11)$$

and $u(z, r) = 0$ for $r \geqq R_b$.

4. The velocity component v throughout the region is obtained by satisfying Eq. (10).

4. Numerical Results

For comparison, three nitrogen arcs will be considered with axis temperatures of 11,000, 12,000, and 13,000 °K. The constrictor tube is maintained at 1,000 °K, and an arc column radius of 0.6 cm is assumed for the first arc which results in a corresponding constrictor radius of 0.79 cm. The transport and the thermodynamic properties are taken from Refs. [11, 12]. The "critical temperature" of nitrogen at atmospheric pressure is approximately 6,000 °K. The field strengths, the currents, and the arc radii obtained from an analysis of the fully developed column are presented, together with the axis temperatures, in Table I. Temperature and current density distributions in the arc column are shown in Figs. 3 and 7, respectively.

Experimental evidence indicates that the thickness of the contraction region is in the order of 0.1 cm. For this analysis, the thickness is assumed to be 0.3 cm. The temperatures on surface D are given by Eq. (5) with the factor $\gamma = 0.2$. The temperature gradients on the anode end of the region are described by Eq. (4) with the gradient $\frac{\partial T}{\partial z}(z_b, R_a) = -2 \times 10^{-4}$ °K/cm. With the region divided into 21 by 41 nodal elements, Eqs. (1) through (11) are solved

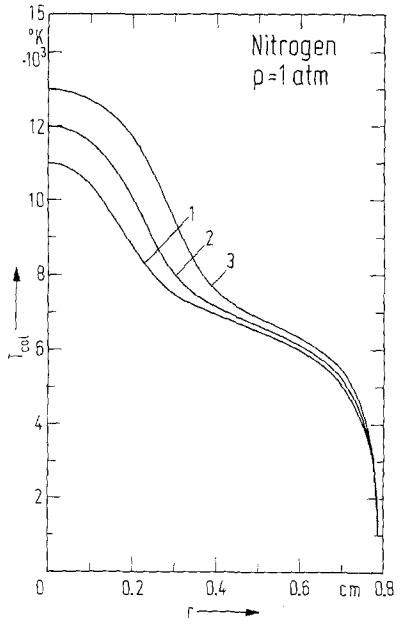

Fig. 3. Temperatures in the Undisturbed Arc Column

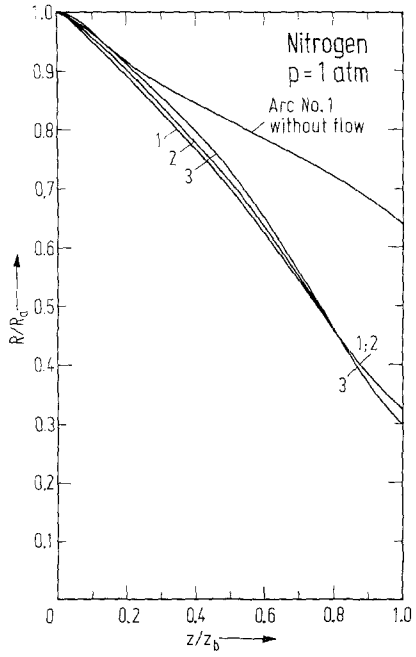

Fig. 4. Arc Peripheries in the Contraction Zone

Table I. Data for fully-developed arcs

Arc	T_0 (°K)	E (volt/cm)	I (amp)	R_a (cm)
1	11,000	9.4	67.9	0.600
2	12,000	8.3	87.7	0.620
3	13,000	7.3	121.4	0.648

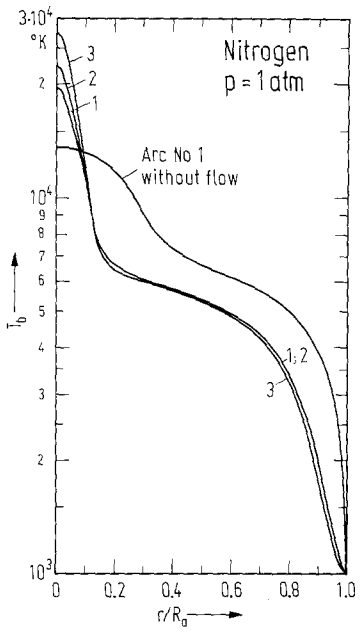

Fig. 5. Temperatures at the Anode End of the Contraction Region (surface B)

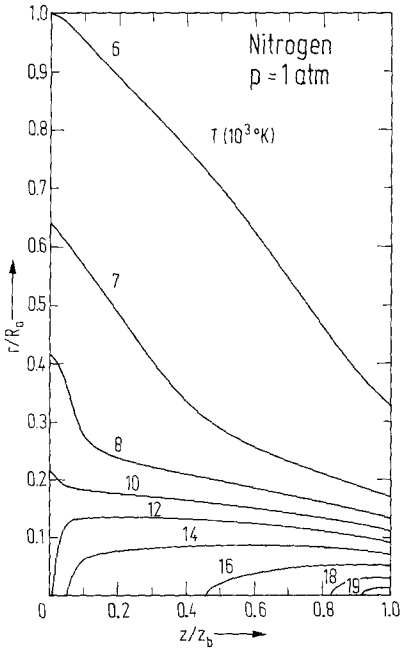

Fig. 6. Isotherms in the Contraction Zone for Arc No. 1

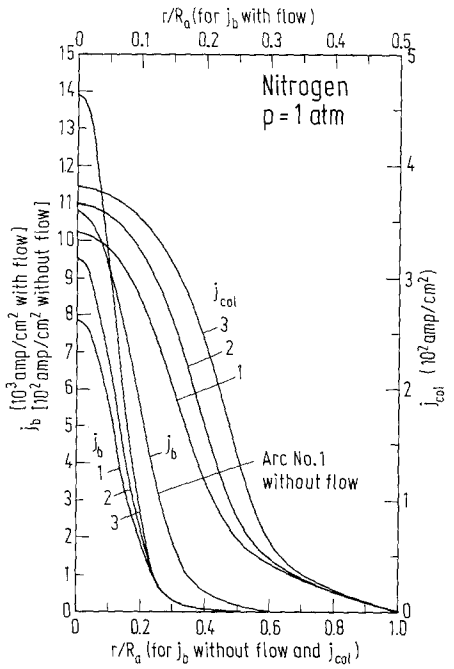

Fig. 7. Current Densities in the Arc Column and at the Anode End of the Contraction Zone

by the Southwell relaxation method [9]. The results obtained for the three cases are shown in Fig. 4 through 10. In order to demonstrate the effect of gas entrainment on the contraction region, the initial constriction without flow is calculated for the first arc. As expected, the contraction is much less severe without flow (Fig. 4); and the peak temperature (Fig. 5) as well as the peak current density (Fig. 7) are substantially lower.

Fig. 8 shows that gas entrainment has also a significant effect on the potential distribution in the contraction region.

Fig. 4 indicates that the radii for all three cases contract to approximately 30 percent of their values on the column end. The arc peripheries show little dependence on current for the current range covered by this investigation although higher currents seem to cause a slightly stronger contraction.

Fig. 5 shows the temperature distribution on the anode end of the contraction region as a function of the dimensionless radius, r/R_a. At $r = R_a$, the three curves meet at a temperature of 1,000 °K which is the assumed low temperature for the surrounding gas. On the inner core, the temperatures are substantially higher and the peak temperatures increase with increasing total current because the current densities increase correspondingly since the current has little effect on the constriction. At the same time, the field strength also increases in this region causing an appreciable increase of the heat dissipation term. Therefore, the rate of heat generation per unit volume is much higher near the anode end of the contraction region. This is consistent with the behavior of the peak temperatures which are strongly affected by the total current (Fig. 5).

In Fig. 6, the isotherms in the contraction region are plotted for arc No. 1. As previously mentioned, the isotherm at 6,000 °K is defined as the arc periphery.

Besides the current density distributions in the column, Fig. 7 also shows those on surface B. The

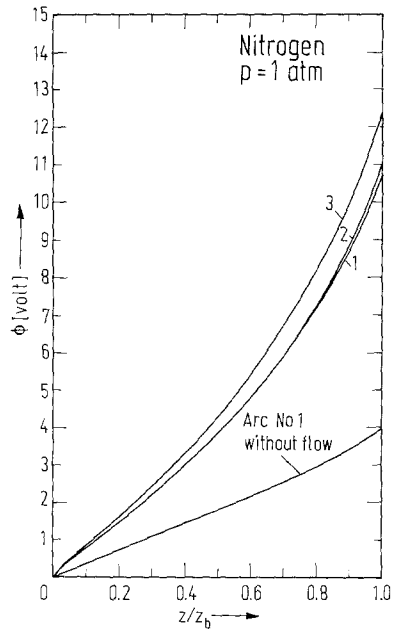

Fig. 8. Potentials on the Center Line of the Contraction Zone

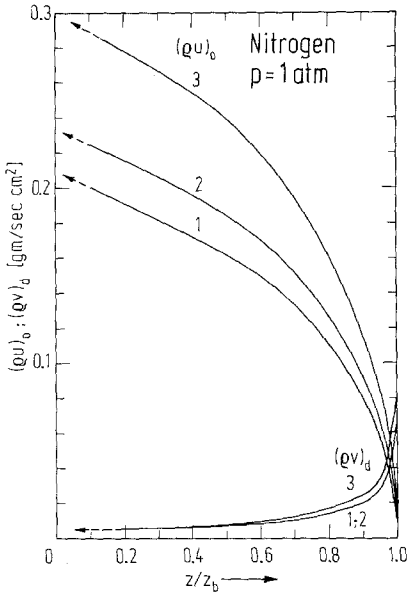

Fig. 9. Axial and Radial Components of the Mass Flow Rate in the Contraction Zone

current densities, as previously discussed, are directly related to the arc currents. For the arcs under consideration, the peak current densities are in the range from 8,000 to 14,000 amp/cm^2, which represents a substantial increase over values typical for the column of confined high intensity arcs.

The electric potentials along the z-axis are shown in Fig. 8 demonstrating that a voltage drop of 10 to 12 volts occurs over the thickness of the contraction region. This voltage drop does not include the anode fall. The equivalent voltage drop in the arc column is between 2 and 3 volts. These numbers illustrate that care must be exercised to experimentally obtain valid values of the anode fall.

In Fig. 9, the axial flow rates on the z-axis, $(\rho u)_0$, and the radial flow rates along the surface D, $(\rho v)_d$, are plotted against the dimensionless distance from the column end. Due to the accumulation of errors, the calculated values are not accurate on the column end ($z = 0$). The dashed lines are approximate extrapolations of the curves on this end. Another illustration of the flow field is provided in Fig. 10 which represents the streamlines of the entrained gas and of the anode jet for the case of arc No. 1.

In order to assess the influence which the most important boundary conditions have on the results, the same calculation is performed with slightly modified boundary conditions. If T_1 is raised from 1000 °K to 3,000 °K, the results show that there is hardly any change in the degree of contraction. The peak temperature, however, decreases by 100 °K.

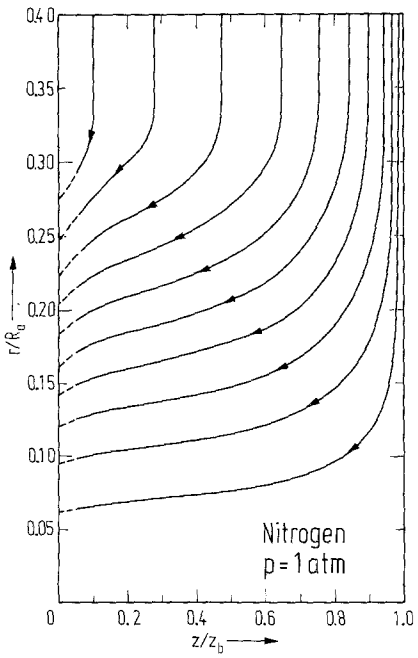

Fig. 10. Stream Lines of the Entrained Gas in the Contraction Region for Arc No. 1

A smaller absolute value of $\frac{\partial T}{\partial z}(z_b, R_a)$ reduces the rate of heat conduction towards the anode; and, consequently, the temperatures in the immediate vicinity of the anode will rise and a similar effect as that observed

for higher T_1 is expected. By choosing $\frac{\partial T}{\partial z}(z_b, R_a) = -15{,}000\,^{\circ}K/cm$, the results show a slightly less severe contraction and a drop of approximately 300 °K in the peak temperature as compared with the original results obtained with $\frac{\partial T}{\partial z}(z_b, R_a) = -20{,}000\,^{\circ}K/cm$.

4. Summary and Conclusions

Based on a simplified model for the anode region of high intensity arcs, the behavior of an atmospheric nitrogen arc in this region has been studied with emphasis on the arc constriction mechanism and the associated spot formation. The results demonstrate that due to the enhanced conduction of heat from the plasma to the low temperature anode surface, the arc contracts in the anode region ("thermal pinch"). This initial constriction leads to a magnetic pumping effect entraining gas from the vicinity of the anode and accelerating this gas in the form of an anode plasma jet towards the cathode. Convective heat transfer due to this entrainment of cold gas represents the predominant constriction mechanism, i. e., the behavior of the arc in the anode region is governed by an energy balance in this region.

In contrast to the situation in a fully-developed arc column where energy and momentum equations are decoupled, the convective term couples in the present case these equations which must be solved simultaneously. This difficult problem has been circumvented in this analysis by employing an approximate solution of the flow field.

The calculated constriction of the arc in the anode region raises the temperature, the electric field strength, and the current density substantially over those prevailing in the adjacent arc column. This fact is considered to be crucial for the formulation of realistic boundary conditions at the interface between contraction zone and anode sheath which, in turn, are necessary for a quantitative anode fall theory.

The high electric field strength in the contraction zone is an indication that direct measurements (for example, by means of potential probes) of the true anode fall are extremely difficult if not impossible. The accuracy and reliability of previous anode fall measurements in this type of arc by means of potential probes or by variation of the arc gap may have suffered from this effect.

Attempts to acquire data in the anode region by the previously-mentioned methods or by employing an energy balance in the anode region and on the anode itself have been reported in the literature [13–25]. None of the reported data permit a direct comparison with the present analysis. Ref. [23] which reports studies in high intensity pulsed arcs in air at atmospheric pressure represents probably the closest approach to the conditions chosen for this analysis. Determination of the spot size for an 80 amp arc resulted in average current densities of approximately 10^4 amp/cm^2 which compares favorably with the peak current density calculated for arc No. 2. The method utilized in Ref. [23] for determining the spot size (from erosion marks) underestimates the width of the actual current density profile so that the reported average current densities are probably close to the peak current densities.

The calculated plasma temperatures in the contraction zone reach values close to $3 \times 10^4\,^{\circ}K$ which makes the assumption of negligible radiation losses in this zone questionable. A refined model must take radiation into account which represents an additional cooling mechanism in the contraction zone.

Another deficiency of the present model becomes obvious if the situation at the interface between plasma column and constriction zone is considered. The flow passing across this surface (Fig. 10) requires an additional transition zone between contraction zone and arc column to allow for a continuous variation and matching of the plasma properties.

The assumption of LTE throughout the contraction zone is another simplification which has to be given up in a more refined model. The relatively high field strength in the contraction region especially towards the sheath edge causes deviations from kinetic equilibrium between electrons and heavy particles. In addition, the high gradients of electrical potential, temperature, and species density may lead to deviations from chemical equilibrium.

The parameter range covered by this study is rather limited. Future work should consider a wider range of arc currents, different gases over a wide range of pressures, and surface effects which inherently enter the picture at higher currents (melting, evaporation).

References

1. Bez, W., Höcker, K. H.: Die Bewegung von Ladungsträgern in nicht-homogenen Feldern. Z. Naturforschg. 9a (1954) 64.
2. Bez, W., Höcker, K. H.: Theorie des Anodenfalls. Z. Naturforschg. 11a (1956) 118.
3. Chou, T.: Anode Contraction Mechanism of High Intensity Arcs. Ph. D. Thesis, University of Minnesota, June, 1971.
4. Ecker, G.: Der Einfluß der Kontraktion auf den Temperatur- und Feldstärkeverlauf vor der Kathode. Z. Physik 132 (1952) 248.
5. Ecker, G.: Die Stabilisierung des Lichtbogens vor Anode und Kathode. Z. Physik 136 (1953) 1.
6. Ecker, G.: Electrode Components of the Arc Discharge. Ergeb. Exakt. Naturw. 33 (1962).
7. Lee, T. H., Greenwood, A. N., Breingan, W. D.: A Self Consistent Model for the Cathode Region of a High Pressure Arc, Proc. Seventh International Conf. on Ionization Phenomena in Gases, Gradevenska Knjega, Beograd, Yugoslavia (1966) 670.

8. Lee, T. H., Greenwood, A. N., Breingan, W. D., Fullerton, H. P.: An Analytical Study of the Physical Processes in the Cathode Region of an Arc. ARL 66-0065 (April, 1966).
9. Schneider, P. J.: Conduction Heat Transfer, Addison-Wesley, Reading, Mass., 1955.
10. Finkelnburg, W., Maecker, H.: Elektrische Bögen und thermisches Plasma. Handbuch der Physik, Bd. XXII, Berlin/Göttingen/Heidelberg: Springer 1956, 254. English translation: ARL 62-302 (1962).
11. Hermann, W., Schade, E.: Transportfunktionen von Stickstoff bis 26 000 °K. Z. Physik 233 (1970) 333.
12. Burhorn, F., Wienecke, R.: Plasmazusammensetzung, Plasmadichte, Enthalpie und spezifische Wärme von Stickstoff, Stickstoffmonoxyd und Luft bei 1, 3, 10 und 30 atm in Temperaturbereich zwischen 1000 und 30 000 °K. Zeitschr. für Physikalische Chemie 215 (1960) 269.
13. Jones, L.: Electrode Evaporation and the Electric Spark. Nature, Lond. 157 (1946) 298.
14. Finkelnburg, W.: Electrode Vapor Jets in Arc and Spark Discharges. Phys. Rev. 74 (1948) 222.
15. Finkelnburg, W.: A Theory of the Production of Electrode Vapor Jets by Sparks and Arcs. Phys. Rev. 74 (1948) 1475.
16. Cobine, J. D., Burger, E. E.: Analysis of Electrode Phenomena in the High-Current Arc. J. Appl. Phys. 26 (1955) 895.
17. Sugawara, M.: Anode Melting Caused by a D.C. Arc Discharge and Its Application to the Determination of the Anode Fall. Brit. J. Appl. Phys. 18 (1967) 1777.
18. Busz-Peuckert, G., Finkelnburg, W.: Die Abhängigkeit des Anodenfalles von Stromstärke und Bogenlänge bei Hochtemperaturbögen. Z. Phys. 140 (1955) 540.
19. Busz-Peuckert, G., Finkelnburg, W.: Zum Anodenmechanismus des thermischen Argonbogens. Z. Phys. 144 (1956) 244.
20. Nestor, O. H.: Heat Intensity and Current Density Distributions at the Anode of High Current, Inert Gas Arcs. J. of Appl. Phys. 33 (1962) 1638.
21. Schoeck, P. A., Eckert, E. R. G.: An Investigation of the Anode Heat Transfer of High Intensity Arcs. Proceedings of the Fifth Internat. Conf. on Ionization Phenomena in Gases, Vol. II, 1812, North-Holland Publishing Comp., Amsterdam, 1962.
22. Finkelnburg, W., Segal, S. M.: High Temperature Plasma Properties from High Current Arc Stream Measurements. Phys. Rev. 80 (1950) 258.
23. Somerville, J. M., Blevin, W. R., Fletcher, N. H.: Electrode Phenomena in Transient Arcs. Proc. Phys. Soc. (London) 65 (1952) 963.
24. Shih, K. T., Pfender, E.: Electrode Energy Transfer Mechanism in an MPD Arc. AIAA Journ. 8 (1970) 211.
25. Bose, T. K., Pfender, E.: Direct and Indirect Measurements of the Anode Fall in a Coaxial Arc Configuration. AIAA Journ. 8 (1969) 1643.

T. S. Chou
Principal Development Engineer
Honeywell, Inc.
Aerospace Division
13350 U.S. Highway 19

E. Pfender, Professor
Heat Transfer Division
Department of Mechanical Engineering
University of Minnesota
Minneapolis, Minnesota 55 455

Received April 5, 1972